



# An analytical representation of raindrop size distribution in a mixed convective and stratiform precipitating system as revealed by field observations

Megumi Okazaki<sup>1</sup>  | Satoru Oishi<sup>2</sup> | Yasuhiro Awata<sup>3</sup> | Tomoro Yanase<sup>4</sup>  | Tetsuya Takemi<sup>5</sup>

<sup>1</sup>Graduate School of Science, Kyoto University, Kyoto, Japan

<sup>2</sup>Research Centre for Urban Safety and Security, Kobe University, Kobe, Japan

<sup>3</sup>Ground Facilities Department, Japan Aerospace Exploration Agency, Tsukuba, Japan

<sup>4</sup>RIKEN Cluster for Pioneering Research, Kobe, Japan

<sup>5</sup>Disaster Prevention Research Institute, Kyoto University, Uji, Japan

## Correspondence

Megumi Okazaki, Disaster Prevention Research Institute, Kyoto University, Gokasho, Uji, Kyoto 611-0011, Japan.  
Email: [okazaki\\_m@storm.dpri.kyoto-u.ac.jp](mailto:okazaki_m@storm.dpri.kyoto-u.ac.jp)

## Funding information

Japan Society for the Promotion of Science, Grant/Award Numbers: 16H04417, 21H01436, 21H01591; JAXA; Furuno Electric

## Abstract

This study investigated a rainfall event under a typhoon influence using a 2D video disdrometer and weather radar observations to characterize raindrop size distribution (DSD) in a mixed convective and stratiform precipitating system. During the time period when both convective and stratiform rainfalls existed, the DSDs generally indicated a monotonically decreasing shape with increasing particle size, with a relatively gradual decrease at intermediate particle size observed at certain times; this feature is attributed to the combined effect of convective and stratiform rainfalls. During the transitional period between convective and stratiform rainfalls, the DSDs exhibited a bimodal shape. The DSDs were well approximated by a newly proposed gamma raindrop distribution combined with exponential (GRACE) distribution function, which was defined as the sum of the exponential distribution and the gamma distribution. A comparison of the volume ratio of the exponential and gamma components of the GRACE distribution revealed that the exponential component of the DSD was larger than the gamma component in the bimodal DSD. These results suggest that the DSD became bimodal during the period when stratiform rainfall predominated because of the weakening of convective rainfall. The GRACE distribution is useful for understanding cloud-microphysical processes in mixed stratiform and convective precipitation conditions.

## KEYWORDS

2DVD, convective rainfall, raindrop size distribution, stratiform rainfall

## 1 | INTRODUCTION

Understanding the raindrop size distribution (DSD) is important to understanding cloud and precipitation phenomena. The DSD represents the number density of raindrops per unit volume with respect to the drop diameter. The moments of a DSD function:

$$m_n \equiv \int_0^{\infty} D^n N(D) dD, \quad (1)$$

are related to precipitation parameters such as the number of particles ( $m_0$ ), water content ( $m_3$ ), and radar reflectivity ( $m_6$ ), where  $N(D)$  represents the number density of raindrops as a function of their diameter  $D$  (e.g.,

This is an open access article under the terms of the [Creative Commons Attribution](https://creativecommons.org/licenses/by/4.0/) License, which permits use, distribution and reproduction in any medium, provided the original work is properly cited.

© 2023 The Authors. *Atmospheric Science Letters* published by John Wiley & Sons Ltd on behalf of the Royal Meteorological Society.

Oishi et al., 2020). The functions commonly used to represent the DSD are the exponential distribution (Marshall & Palmer, 1948),

$$N(D) = N_0 \exp(-\Lambda D), \quad (2)$$

and the gamma distribution (Ulbrich, 1983),

$$N(D) = N_0 D^\mu \exp(-\Lambda D), \quad (3)$$

where  $N_0$ ,  $\Lambda$ , and  $\mu$  denote the intercept, slope, and shape parameters, respectively (Tokay et al., 2008). When  $\mu = 0$ , Equation (3) is identical to Equation (2).

The characteristics of a DSD are known to vary depending on the rainfall pattern. In particular, the DSD shape differs between stratiform and convective rainfalls (e.g., Niu et al., 2010; Seela et al., 2017; Tokay & Short, 1996). Wu and Liu (2017) showed that DSDs were linked to regional rainfall differences as well as differences in stratiform and convective characteristics. Atlas et al. (1999) have suggested that the gamma distribution is representative of convective rainfall, whereas the exponential distribution is representative of stratiform rainfall.

Mixed stratiform and convective precipitating states can be found in mesoscale precipitation systems. Houze et al. (1989) conceptually depicted an example of such a precipitating system. Shusse et al. (2009) presented, from radar observations, the characteristics of convective rainfall embedded within stratiform rainfall in a Baiu front environment. Stratiform rainbands are also generated by active convection within a tropical cyclone (Didlake & Houze, 2013). Das et al. (2017) showed that, in a mixed convective and stratiform system, the DSD became bimodal. Radhakrishna and Rao (2009) observed a bimodal DSD during the transition between convective and stratiform rainfalls in VHF-band radar observations.

Bimodal DSDs show a maximum number of raindrops with a small diameter and a secondary peak at an intermediate diameter. Such bimodal DSDs are generated through collision and breakup via cloud microphysical processes (e.g., D'addario et al., 2015; Konwar et al., 2014; Luo et al., 2020; Prat & Barros, 2007). Cecchini et al. (2014) emphasized the importance of the collection (e.g., collision-coalescence) process in forming a bimodal DSD. Luo et al. (2020) found that DSDs were observed during the passage of convective rainfall cells when collisional breakup occurred. Mallet and Barthes (2009) suggested that the gamma distribution is not an appropriate model function for a DSD with multiple local peaks. Thurai and Bringi (2018) showed that a generalized gamma distribution with more flexibility of parameters than the gamma distribution indicated in Equation (3)

well represented the equilibrium DSD. However, there has not been sufficient discussion on functions that can successfully represent complex DSDs, such as those with bimodal characteristics.

A well-known phenomenon of mixed precipitation features is the seeder–feeder effect (e.g., Misumi et al., 2021; Rutledge & Hobbs, 1983). Misumi et al. (2021) demonstrated the vertical process of the seeder–feeder effect in convective clouds with a melting layer by analyzing typhoon observations. Ahmad et al. (2020) showed that a couple of precipitation cells merged to form a system of multiple cells having various precipitation features.

We considered that DSDs whose shapes were difficult to represent with conventional functions because of their characteristic slope changes at intermediate diameters (e.g., the bimodal form) were produced by composition of two precipitation systems and could be represented by the sum of two functions. Therefore, we define the following function as the sum of the exponential distribution and the gamma distribution:

$$N_{\text{GRACE}}(D) \equiv N_1 \exp(-\Lambda_1 D) + N_2 D^{\mu_2} \exp(-\Lambda_2 D). \quad (4)$$

Equation (4) is called the gamma raindrop distribution combined with exponential (GRACE) distribution. We demonstrate that the GRACE distribution is useful for representing the observed DSDs. We further use this function to characterize the DSD brought by a mixed system of stratiform and convective clouds observed in the Japan region. Herein, we report an observational case for a rainfall event that occurred under the influences of Typhoon Mindulle (2021) by utilizing continuous observations data by a 2D video disdrometer (2DVD) with a high temporal frequency as well as a dual-polarization Doppler radar. These simultaneous observations are useful in evaluating the rainfall process (e.g., Bringi et al., 2003; Sheppard & Joe, 1994; Thurai et al., 2021).

## 2 | DATA AND METHODS

### 2.1 | Data

Observation data were obtained using 2DVD and dual-polarization Doppler radar located in Katsuura, Chiba Prefecture, Japan (Figure 1a).

A 2DVD is a ground-based disdrometer that measures the size, shape, and fall velocity of raindrops (Kruger & Krajewski, 2002), and this information is useful in determining the DSD (e.g., Cao et al., 2008; Marzuki et al., 2010; Tokay et al., 2001; Tokay et al., 2013). Precipitation particles were classified into 56 bins ranging from 0.2 to 5.7 mm in equivolume diameter at 0.1 mm

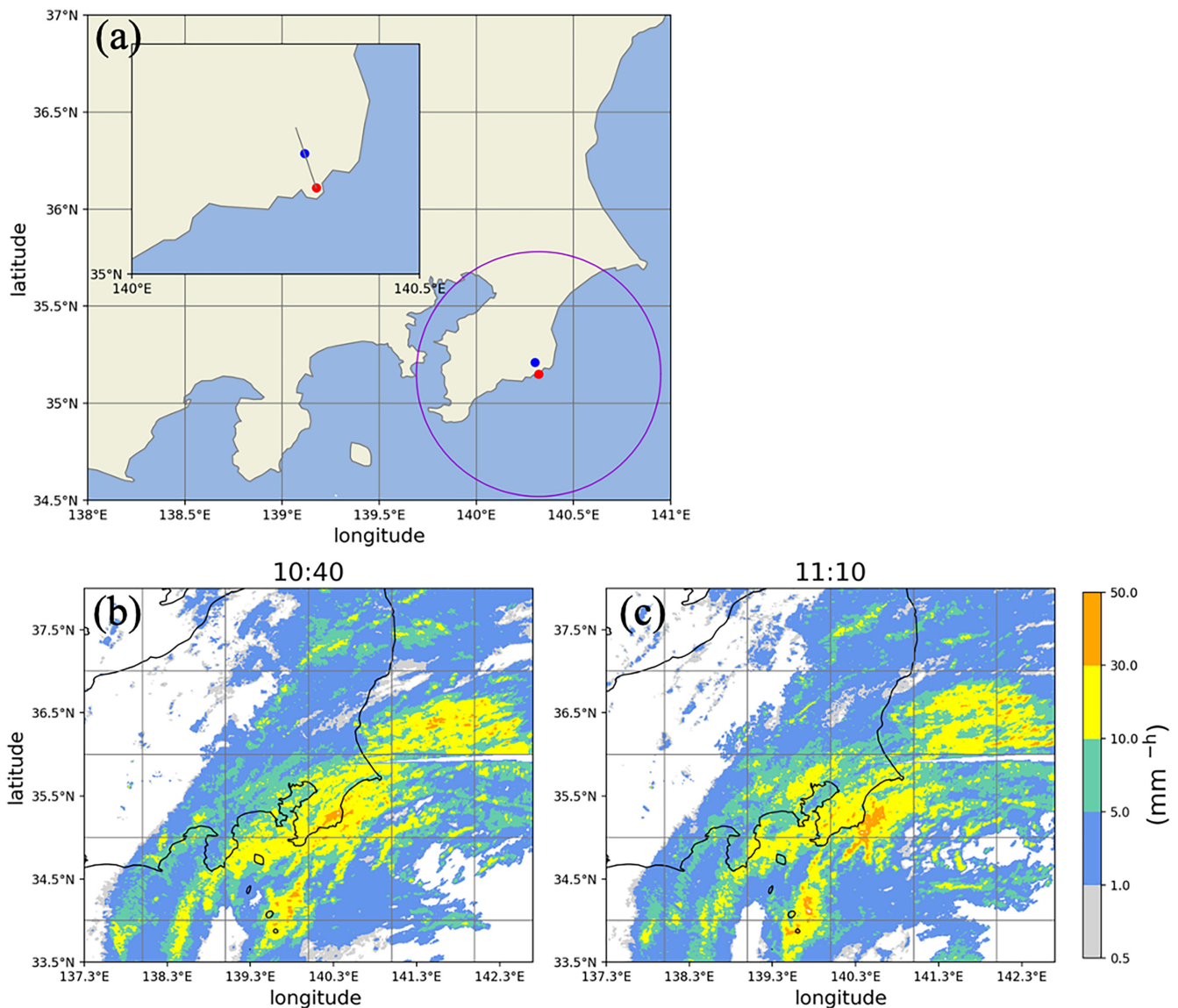


**FIGURE 1** (a) Locations of dual-polarization Doppler radars ( $35.15^{\circ}\text{N}$ ,  $140.32^{\circ}\text{E}$ ; red point) and 2D video disdrometer ( $35.21^{\circ}\text{N}$ ,  $140.30^{\circ}\text{E}$ ; blue point) at Katsuura in Chiba Prefecture, the radar-observable range (purple circle), and observation area of the sector scanning of range height indicator (SRHI) scan in this study (gray line). (b,c) Rainfall intensity ( $\text{mm h}^{-1}$ ) in the Kanto region, as obtained from the JMA radar echo composite on October 1, 2021 at (a) 10:40 and (b) 11:10 Japan Standard Time.

intervals. In this case, the diameter  $D$  represented the maximum size of each particle class. Rainfall amounts were measured at 1 min intervals. Time indicated that the observation was made in the previous minute. For example, the observation from 10:00 (HH:MM) to 10:01 is defined as the data at 10:01. The 2DVD was operated by the Japan Aerospace Exploration Agency (JAXA) and was installed at a location in Katsuura ( $35.21^{\circ}\text{N}$ ,  $140.30^{\circ}\text{E}$ ) at an altitude of  $\sim 150$  m.

We used a dual-polarization Doppler radar located at the City Hall of Katsuura ( $35.15^{\circ}\text{N}$ ,  $140.32^{\circ}\text{E}$ ). The radar uses dual polarization and its frequency is 9.4 GHz (X-band). The peak output power is 100 W, the beam width is  $2.7^{\circ}$ , and the antenna rotation rate is 6.0 rpm. The pulse width is 9  $\mu\text{s}$ ,

the pulse repetition frequency is 800.0–1000.0 Hz, and the range resolution is 100 m. The radar has an observable radius of 70 km (Figure 1a). In this study, we examined observation data obtained by sector scanning of range height indicator (SRHI). The azimuth angle was fixed at  $344^{\circ}$ , which was directed toward the 2DVD site, which was located  $\sim 7$  km from the radar. Like the 2DVD data, the rainfall data were obtained at 1 min intervals. The time display in a 1 min radar observation was the beginning of the observation. For example, results obtained during the 1 min period from 10:00 to 10:01 were defined as 10:00 time data.

Rainfall characteristics are represented by the following radar parameters. Parameter  $\rho_{\text{HV}}$  indicates the fluctuation of the ratio of the horizontal and vertical lengths of

particles, which is smaller when different types of particles coexist or when distorted particles, such as individual particles, are present (Fukao & Hamazu, 2014). Parameter  $Z_{DR}$  depends on the ratio between the horizontal and vertical lengths of the precipitation particles, and its value increases with increasing diameter in case of raindrops (Fukao & Hamazu, 2014). Parameter  $Z_{HH}$  is the radar reflection intensity at horizontal polarization, expressed as the sixth moment of the number distribution (Equation 3; Rauber & Nesbitt, 2018). Parameter  $K_{DP}$  depends on the number concentration and particle oblateness, with larger values for larger raindrops (Rauber & Nesbitt, 2018). We have corrected the attenuation of  $Z_{HH}$  and  $Z_{DR}$  to raindrops using  $K_{DP}$ , following Maesaka et al. (2011).

## 2.2 | Method of analysis with GRACE distribution

We analyzed observation data obtained by 2DVD to show that the GRACE distribution can accurately represent DSDs in an environment where stratiform and convective rainfalls coexist. To obtain a robust feature for DSD, we took moving averages among the neighboring three drops size bins. The least-squares method was used to obtain a fitting function. Modules from the *scipy* library (version 1.9.0; Virtanen et al., 2020) were used to obtain an analytical function that fits the observed DSDs from a least-squares method. In the least-squares method, the model function (i.e., the GRACE distribution) used to approximate the observed DSD was approached by minimizing the square of the error for each size class. The number density of particles with large diameters is considerably smaller than that of particles with small diameters. Thus, a fitting curve from the least-squares method will be strongly affected by the large number of smaller particles and cannot represent the number density of the largest particles. We therefore evaluated the errors as water content by weighting with the third power of the diameter for each particle bin. Here, an analysis was performed using the least-squares method with the number density distribution of the  $i$ th class  $N(D_i)$  multiplied by the third power of the particle size of the  $i$ th class  $D_i$ ,

$$\sum_{i=1}^n (N_{GRACE}(D_i)D_i^3 - N(D_i)D_i^3)^2, \quad (5)$$

where  $n$  is the total number of drop-size classes, which here is 54. The function was determined by minimizing Equation (5) with the five parameters of the GRACE distribution as variables. The root mean square error (RMSE) value expressed by the following equation was used as a measure of the accuracy of the fitting:

$$RMSE = \sqrt{\frac{1}{n} \sum_{i=1}^n (N_{GRACE}(D_i)D_i^3 - N(D_i)D_i^3)^2}. \quad (6)$$

The RMSE value is an index that is smaller when the model function is closer to the observed value. Because this analysis method requires the establishment of a range of values within which the variables can change, a range was established for each of the five parameters of the GRACE distribution. In order to improve the estimation of the parameters with the lowest RMSE, the upper limit of the scope of parameters searching was varied by trial and error in order for the RMSE values to become smaller while the lower limit was set to zero. We performed a similar analysis using the gamma distribution (Equation (3)) and compared the results with the RMSE values obtained from the GRACE distribution analysis to examine which distribution was more appropriate to represent the DSDs of mixed stratiform and convective rainfall systems.

## 2.3 | An analyzed case: Typhoon Mindulle (2021)

Typhoon Mindulle hit the south of Chiba Prefecture at 10:00–11:00 Japan Standard Time (JST) on October 1, 2021 (Figure 1b,c). These data of Figure 1b,c obtained from the Japan Meteorological Agency (JMA) radar echo composite (Atmosphere and Ocean Department of JMA, 2021). The average wind direction in Katsuura was north–northeast at 10:00 and north at 11:00 JST according to JMA surface observations. The data indicate that the local precipitation system was moving in the direction of the SRHI azimuth closer to the radar. Because of typhoon rainbands, the highest daily precipitation of 35.0 mm h<sup>-1</sup> was observed at Katsuura in 1 h between 10:00 and 11:00 JST according to JMA surface observations. Rainfall brought by tropical cyclones contains high concentrations of small and medium raindrops and has similar distribution to continental thunderstorms (Tokay et al., 2008). For the typhoon case, the spectral width of particle size about the DSD observed in the outer rain band was larger than in the shallow convection, on the other hand, the number density of smaller sized particles was larger in the shallow convection than in the outer rain band (Bao et al., 2019).

## 3 | OBSERVATIONS WITH 2DVD AND RADAR

Figure 2 shows the temporal variation of the radar parameters and 2DVD rainfalls from 10:30 to 11:30. The radar

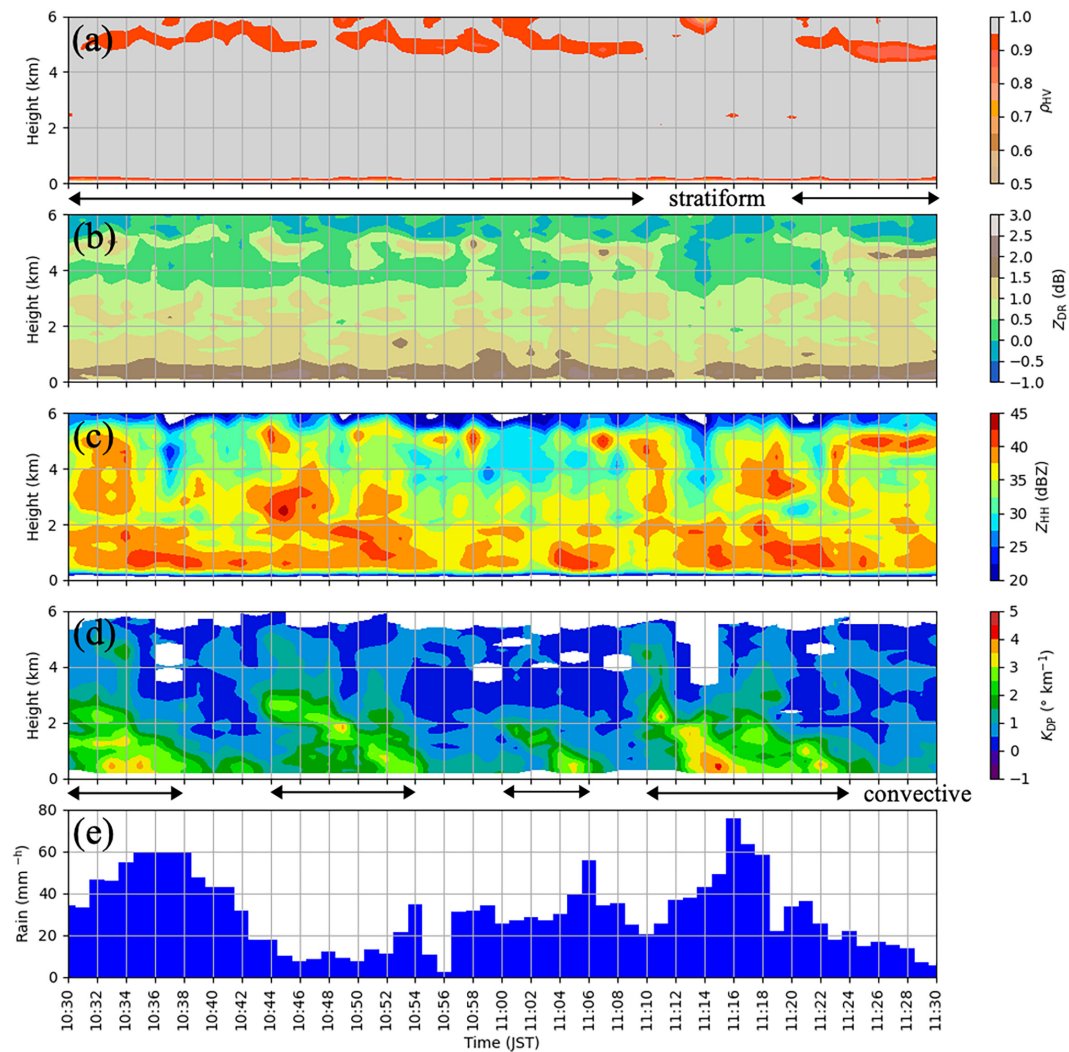


**FIGURE 2** Time–height diagram of radar observation parameters (a)  $\rho_{HV}$ , (b)  $Z_{DR}$ , (c)  $Z_{HH}$ , and (d)  $K_{DP}$  from 10:30 to 11:30 Japan Standard Time (JST). The horizontal average is in the  $1 \text{ km}^2$  region centered on the 2D video disdrometer (2DVD) observation location. (e) The rainfall intensity measured using a 2DVD at the same time.

parameters shown in Figure 2a–d were observed at 6500–7500 m from the radar site and averaged for the data vertically at 100 m intervals, which means observation area of the upper air of the 2DVD. In the layers at  $\sim 5 \text{ km}$  altitude,  $\rho_{HV}$  was  $< 0.95$  and  $Z_{DR}$  was  $> 0.5 \text{ dB}$  at  $\sim 10:30$ – $11:10$  and  $11:20$ – $11:30$  (Figure 2a,b). According to the analysis fields from the operational mesoscale numerical weather prediction model, the Meso-Scale Model, of JMA revealed that the melting layer altitude at 12:00 in Chiba Prefecture was  $\sim 5 \text{ km}$  (Information Infrastructure Department of JMA, 2022). This situation indicates the presence of bright bands, suggesting that a stratiform system within the typhoon rainbands was widespread over the 2DVD site. On the other hand, it was difficult to see the bright bands in  $Z_{HH}$  (Figure 2c). This may reflect the need for more sophisticated attenuation correction.

Regions with  $K_{DP} > 2.5^\circ \text{ km}^{-1}$  existed below  $\sim 2 \text{ km}$  at 10:30–10:38, 10:44–10:54, 11:00–11:06, and 11:10–11:24 (Figure 2d). These areas were observed to move downward at a rate of  $\sim 300 \text{ m min}^{-1}$  between 10:44 and 10:54. This observation indicates that raindrops with larger sizes were dominant and fell with a speed of  $5 \text{ m s}^{-1}$ . The results suggest that convective cells within the rain band were present during these time periods.

Convective rainfall was observed on the ground, with rainfall intensity of  $40 \text{ mm h}^{-1}$  or greater at 10:32–10:41, 11:05, 11:06, and 11:14–11:18 in the 2DVD (Figure 2e). A strong region of  $K_{DP}$  was also observed at 10:44–10:54; however, despite increasing rainfall intensity at 10:54, this convective cell appears to not correspond to stronger surface rainfall. Moreover, although the rainfall area with a  $K_{DP}$  of  $2.5^\circ \text{ km}^{-1}$  existed from 11:10 to 11:24, surface

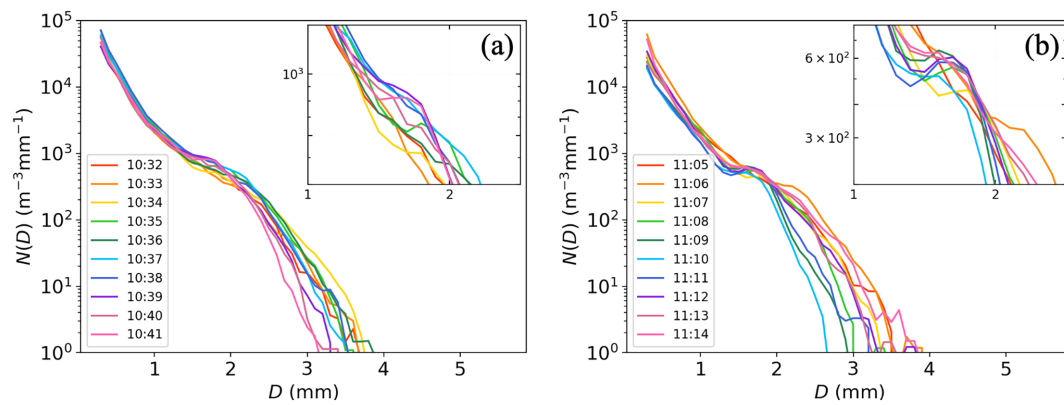


**FIGURE 3** Raindrop size distribution per minute (a) from 10:32 to 10:41 and (b) from 11:05 to 11:14 Japan Standard Time (JST), as measured using 2D video disdrometer. The upper-right box shows the raindrop particle size distribution expanded over the range from 1 to 2.5 mm in diameter.

rainfall intensity  $>40 \text{ mm h}^{-1}$  was observed from 11:14 to 11:18 and ended earlier in the 2DVD than in the  $K_{DP}$  signature. As previously mentioned, there were periods of slightly different times for convective rainfall observed on the ground and convective clouds in the upper air. However, given that the precipitation system moved in three dimensions and that the detailed analysis was conducted at intervals as short as 1 min, the response was generally adequate. Therefore, rainfall  $>40 \text{ mm h}^{-1}$  that lasted 2–10 min during stratiform rainfall having an intensity  $<20 \text{ mm h}^{-1}$  can be considered to be the result of convective clouds embedded within stratiform clouds. From 11:04 to 11:08,  $Z_{HH}$  was  $>30 \text{ dBZ}$  at  $\sim 5 \text{ km}$  because of the presence of the bright band and was  $>35 \text{ dBZ}$  below 3 km because of convective activity. The vertical structure of  $Z_{HH}$  appears to be similar to a feature that Shusse et al. (2009) found in precipitating convective clouds embedded within stratiform clouds.

Given the aforementioned observations, we focus on the DSD from 10:32 to 10:41, which is the time between the overlap of convective and stratiform rainfalls and the end of convective rainfall. We also focus on the DSD from 11:05 to 11:14, which corresponds to the time between the overlap of convective and stratiform rainfalls, the end of convective rainfall, and the beginning of the next convective rainfall.

To characterize the shape of the DSD, the minute-by-minute DSDs at 10:32–10:41 and 11:05–11:14 are shown in Figure 3a,b, respectively. Because of fluctuations in the observed values for each diameter class, we here show the DSD obtained by taking the moving averaged over the three classes in diameter to demonstrate robust characteristics. At 10:32–10:34, 10:36–10:40, 11:05, 11:06, 11:13, and 11:14, the number density distribution appears to decrease monotonically with increasing diameter, with the rate of decrease stagnating at intermediate particle

sizes (Figure 3). These time periods correspond to periods of heavy rainfall due to both stratiform and convective precipitation (Figure 2). In particular, at 10:35, 10:41, 11:07, 11:08, 11:09, 11:11, and 11:12, each peak in the 1–2 mm class was found to be a bimodal type. At 11:10, no substantial peak was observed; however, the distribution approximated a bimodal form. Figure 2f shows that the rainfall intensity was weakening at 10:41, 11:07, 11:08, 11:09, and 11:10 and strengthening at 11:11 and 11:12. The decrease in rainfall intensity at 10:41, 11:07, 11:08, 11:09, and 11:10 was due to the weakening of rainfall from convective cells embedded in stratiform rainfall present at 10:30–10:38, 11:00, and 11:06 (Figure 2). Moreover, the intensity of the subsequent convective rainfall started to increase at 11:11 and 11:12 (Figure 2d,f). Therefore, the DSD clearly became bimodal during the transition process between stratiform and convective rainfalls. The results support the assertion of Radhakrishna and Rao (2009) that a bimodal DSD was observed during the transition between convective and stratiform rainfalls. However, at 10:35, a bimodal distribution was observed without a clear transition between stratiform and convective rainfalls. At this time, the bimodal distribution may appear in between the active convective cores.

#### 4 | AN ANALYTICAL REPRESENTATION FOR DSD: GRACE DISTRIBUTION

The results of fitting to the DSDs at 10:32–10:41 and 11:05–11:14 show that the GRACE distributions fairly well approximated the observed DSDs at each time (Figure 4). In the analysis at 11:09, the parameter numbers of  $N_2$  and  $\Lambda_2$  became too large and reached the upper limit of the possible range of motion.

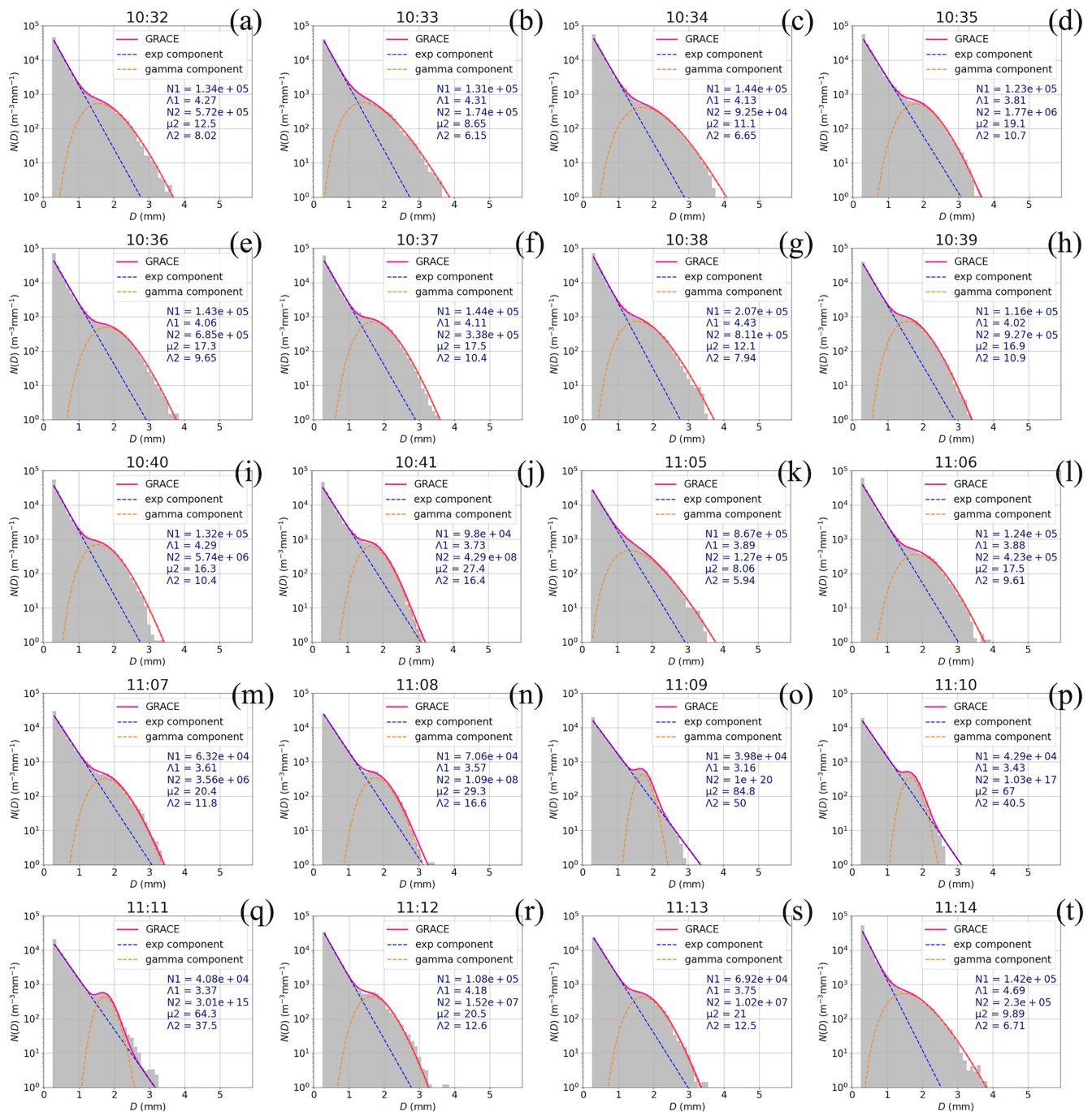


**FIGURE 4** The results of fitting of gamma raindrop distribution combined with exponential (GRACE) distribution to moving-average raindrop size distribution for three diameter classes per minute, as measured using 2D video disdrometer: (a–j) 10:32–10:41 and (k–t) 11:05–11:14 Japan Standard Time. Silver histograms, pink solid lines, blue-dotted lines, and orange-dotted lines represent observational data, the GRACE distribution, the exponential component of the GRACE distribution, and the gamma distribution component of the GRACE distribution, respectively. The parameters of the GRACE distribution are written in navy.

Figure 5a,b show the time variation of the RMSE obtained from the analysis of the GRACE, exponential distributions, and gamma distributions. The RMSE values were generally smaller in the GRACE distribution analysis than in the exponential distribution and the gamma distribution analysis. These

results clarify that the GRACE distribution is more useful than the conventional exponential or gamma distribution.

To further examine the usefulness of the GRACE distribution to describe the DSD features, we compared the ratio of the exponential and gamma function components

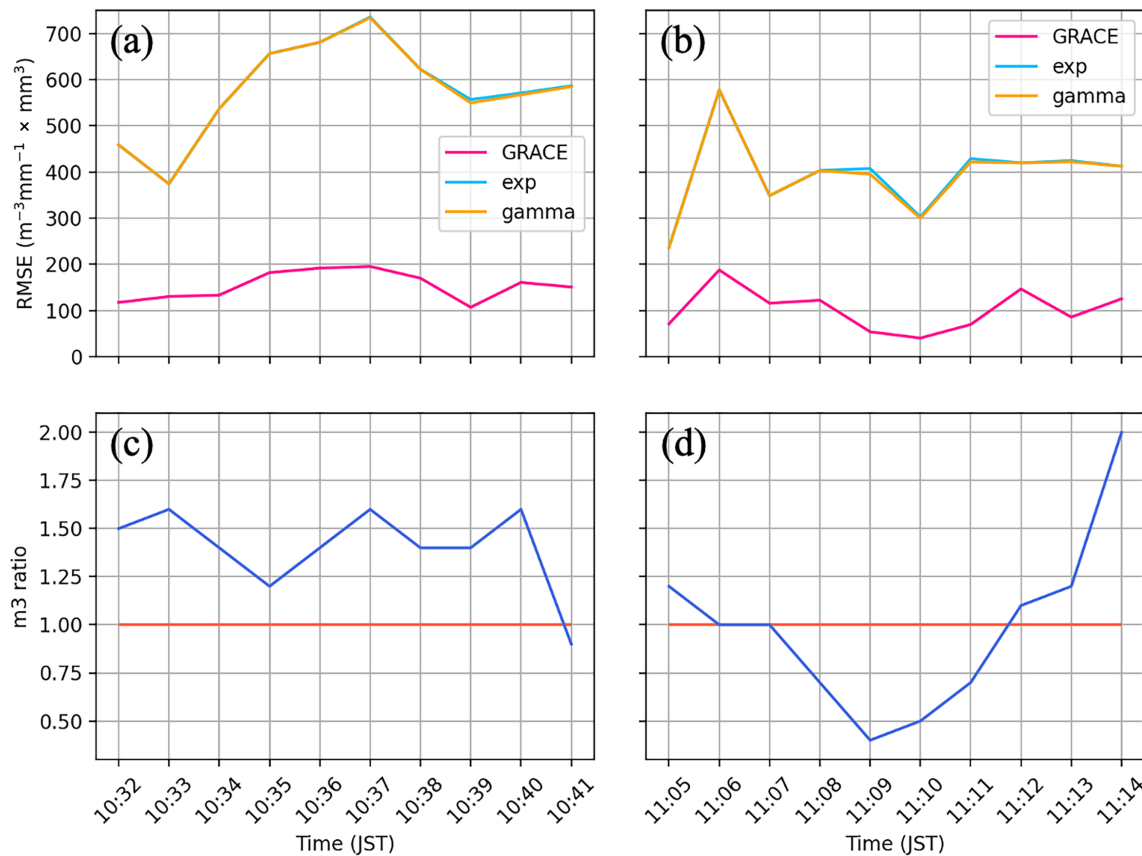


**FIGURE 5** (a,b) Time series about the root mean square error (RMSE) value between observational raindrop size distributions (DSDs) and the gamma raindrop distribution combined with exponential (GRACE) distribution, the exponential distribution, and the gamma distribution (a) from 10:32 to 10:41 and (b) from 11:05 to 11:14 Japan Standard Time (JST). (c,d) Ratio of the third moment between the exponential and gamma components of the GRACE distribution (c) from 10:32 to 10:41 and (d) from 11:05 to 11:14 JST.

of the GRACE distribution for each time period. The third moment of the number distribution was used for comparison (Equation 1). The third moments of the DSD for the exponential and gamma parts of the GRACE distribution, respectively, were calculated using the following equation:

$$\text{m3ratio} = \frac{\int_0^{\infty} D^3 N_2 D^{\mu_2} \exp(-\Lambda_2 D) dD}{\int_0^{\infty} D^3 N_1 \exp(-\Lambda_1 D) dD}. \quad (7)$$

If the ratio of the third moment has a value of 1, the exponential and gamma components of the GRACE distribution have equal contributions. If the value exceeds 1, the gamma component of the GRACE distribution has a greater contribution.

Figure 2 shows that strong rainfall due to the superposition of stratiform and convective rainfalls occurred at 10:32–10:40, 11:05–11:06, and 11:13–11:14. In these time periods, the m3ratio exceeded 1 (Figure 5c,d). Given that the gamma component of the GRACE distribution is

representative of convective rainfall, these results suggest that convective rainfall was more dominant than stratiform rainfall during these times. However, at 10:41 and 11:07–11:12, the m3ratio was <1. At 10:41, 11:07–11:09, and 11:11–11:12, in particular, the DSD was bimodal. During these times, convective rainfall weakened and stratiform rainfall predominated. The increases in  $\mu_2$  and  $\Lambda_2$  of the fitting parameters for these times compared with the time before and after correspond to a smaller width of the gamma distribution in the GRACE distribution (Figure 4). At 11:05 and 11:06, convective rainfall was embedded in the stratiform rainfall and the addition of the two types of rainfall might have caused a relatively gentle slope in the intermediate diameter range of the DSDs (Figures 2a–d, 3, 4, and 5d). Convective rainfall then decreased from 11:07 to 11:10, and a bimodal DSD was observed. In particular, the time evolution of the m3ratio in Figure 5d suggests that the convective rainfall embedded in the stratiform rainfall at 11:05 and 11:06 gradually decreased from 11:07 to 11:10 and then increased with the appearance of the next convective rainfall from 11:11.



Notably, at 10:35, the m3ratio was  $>1$ , suggesting that the number distribution should be more strongly affected by the gamma distribution in our proposed formula. However, the distribution at 10:35 exhibits a bimodal feature (Figure 3a). Since there were some cases that could not be evaluated by the m3ratio, it is necessary to increase the number of samples and to conduct a statistical analysis in a future study.

## 5 | CONCLUSIONS

In this study, we proposed a novel approximation function and investigated the DSD features within a precipitation system of mixed convective and stratiform rainfalls. The conclusions of this study are summarized as follows:

- When compared with the gamma distribution, the GRACE distribution, which is composed of the exponential distribution and the gamma distribution added together, more accurately represented DSDs with characteristic slope changes at intermediate diameters.
- In a precipitation system where convective and stratiform rainfalls coexisted, the overlap of convective and stratiform rainfalls formed a DSD that monotonically decreases in diameter from the smallest particle size density, with the slope of the decrease becoming smaller at intermediate diameters.
- When convective rainfall decreased from a rainfall profile where convective and stratiform rainfalls combined, and stratiform rainfall became dominant, the DSD became bimodal, with a peak at the intermediate particle size.

The range of observations covered in this study is limited, and future analyses on a larger number of cases than this one should be conducted to investigate the generality of these theories. Although this study focused on a typhoon rainband, the result obtained should be applied to other mesoscale precipitating systems, which have both convective and stratiform clouds. Mechanisms regarding cases that differ from these conclusions need to be identified. The cloud physical formation factors of DSDs obtained from precipitation systems with mixed convective and stratiform rainfalls need to be clarified. The GRACE distribution was proposed as a function of the sum of the exponential and gamma distributions, but it should be considered to investigate the use of the normalized gamma instead of the gamma distribution, to represent the observations more respectfully than the present GRACE distribution (Illingworth & Blackman, 2002). In addition, the use of the GRACE distribution, the usefulness of which was demonstrated in this study, is expected to enable accurate representations of rainfall

intensity and cloud precipitation parameters in the model for precipitation systems with mixed convective and stratiform precipitations.

## AUTHOR CONTRIBUTIONS

**Megumi Okazaki:** Conceptualization; data curation; formal analysis; investigation; methodology; project administration; visualization; writing – original draft. **Satoru Oishi:** Funding acquisition; methodology; resources. **Yasuhiro Awata:** Data curation; resources; software. **Tomoro Yanase:** Methodology; software; validation. **Tetsuya Takemi:** Funding acquisition; supervision; writing – review and editing.

## ACKNOWLEDGMENTS

The authors would like to thank anonymous reviewers for their comments which are useful in improving the original article. They thank the Katsuura municipal government for allowing us to conduct research in Katsuura, Chiba Prefecture. This work was supported by JSPS KAKENHI (Grant Numbers 16H04417, 21H01436, and 21H01591). JAXA, Furuno Electric, and Kobe University supported the weather observations.

## DATA AVAILABILITY STATEMENT

Radar echo composite data and Meso-Scale Model data of JMA were obtained from the Global Atmospheric Observation Data server of Research Institute for Sustainable Humanosphere, Kyoto University at <http://database.rish.kyoto-u.ac.jp/arch/jmadata/data/jma-radar/synthetic/original/> and at <http://database.rish.kyoto-u.ac.jp/arch/jmadata/data/gpv/netcdf/>, respectively.

## ORCID

Megumi Okazaki  <https://orcid.org/0000-0003-3851-5977>

Tomoro Yanase  <https://orcid.org/0000-0003-2788-9092>

## REFERENCES

- Ahmad, F., Yamaguchi, K. & Nakakita, E. (2020) Investigation of single cell to multicell in the cluster thunderstorms using vorticity analysis. *Journal of Japan Society of Civil Engineers, Series B, (Hydraulic Engineering)*, 76, 187–192.
- Atlas, D., Ulbrich, C.W., Marks, F.D., Amitai, E. & Williams, C.R. (1999) Systematic variation of drop size and radar-rainfall relations. *Journal of Geophysical Research*, 104, 6155–6169.
- Atmosphere and Ocean Department of JMA. (2021) On the provision of 5 minutes intervals 250 m mesh nation-wide composited radar precipitation intensity GPV, *Technical Information*, No. 568, 48 pp (in Japanese). Available at: <https://www.data.jma.go.jp/suishin/jyouhou/pdf/568.pdf> [Accessed 20th December 2022].
- Bao, X., Wu, L., Tang, B., Ma, L., Wu, D., Tang, J. et al. (2019) Variable raindrop size distributions in different rainbands

- associated with typhoon Fitow (2013). *Journal of Geophysical Research. Atmospheres*, 124, 12262–12281.
- Bringi, V.N., Chandrasekar, V., Hubbert, J., Gorgucci, E., Randeu, W. L. & Schoenhuber, M. (2003) Raindrop size distribution in different climatic regimes from disdrometer and dual-polarized radar analysis. *Journal of the Atmospheric Sciences*, 60, 354–365.
- Cao, Q., Zhang, G., Brandes, E., Schuur, T., Ryzhkov, A. & Ikeda, K. (2008) Analysis of video disdrometer and polarimetric radar data to characterize rain microphysics in Oklahoma. *Journal of Applied Meteorology and Climatology*, 47, 2238–2255.
- Cecchini, M.A., Machado, L.A.T. & Artaxo, P. (2014) Droplet size distribution as a function of rainy system type and cloud condensation nuclei concentrations. *Atmospheric Research*, 143, 301–312.
- D'Adderio, L.P., Porcù, F. & Tokay, A. (2015) Identification and analysis of collisional breakup in natural rain. *Journal of the Atmospheric Sciences*, 72, 3404–3416.
- Das, S.K., Konwar, M., Chakravarty, K. & Deshpande, S.M. (2017) Raindrop size distribution of different cloud types over the Western Ghats using simultaneous measurements from micro-rain radar and disdrometer. *Atmospheric Research*, 186, 72–82. Available from: <https://doi.org/10.1016/j.atmosres.2016.11.003>
- Didlake, A.C., Jr. & Houze, R.A., Jr. (2013) Dynamics of the stratiform sector of a tropical cyclone rainband. *Journal of the Atmospheric Sciences*, 70, 1891–1911.
- Fukao, S. & Hamazu, K. (2014) *Radar for meteorological and atmospheric observations*. Tokyo: Springer.
- Houze, R.A., Jr., Rutledge, S.A., Biggerstaff, M.I. & Smull, B.F. (1989) Interpretation of doppler weather radar displays of mid-latitude mesoscale convective systems. *Bulletin of the American Meteorological Society*, 70, 608–619.
- Illingworth, A.J. & Blackman, T.M. (2002) The need to represent raindrop size spectra as normalized gamma distributions for the interpretation of polarization radar observations. *Journal of Applied Meteorology and Climatology*, 41, 286–297.
- Information Infrastructure Department of JMA. (2022) On the extension of forecast time of MSM/LFM GPV and MSM guidance, *Technical Information*, No. 500, 40 pp (in Japanese). Available at: <https://www.data.jma.go.jp/suishin/jyouhou/pdf/500.pdf> [Accessed 20th December 2022].
- Konwar, M., Das, S.K., Deshpande, S.M., Chakravarty, K. & Goswami, B.N. (2014) Microphysics of clouds and rain over the Western Ghat. *Journal of Geophysical Research. Atmospheres*, 119, 6140–6159.
- Kruger, A. & Krajewski, W.F. (2002) Two-dimensional video disdrometer: A description. *Journal of Atmospheric and Oceanic Technology*, 19, 602–617.
- Luo, L., Xiao, H., Yang, H., Chen, H., Guo, J., Sun, Y. et al. (2020) Raindrop size distribution and microphysical characteristics of a great rainstorm in 2016 in Beijing, China. *Atmospheric Research*, 239, 104895. Available from: <https://doi.org/10.1016/j.atmosres.2020.104895>
- Maesaka, T., Maki, M., Iwanami, K., Tsuchiya, S., Kieda, K. & Hoshi, A. (2011) Operational rainfall estimation by X-band MP radar network in MLIT, Japan. Proceedings of 35th conference on radar meteorology, Pittsburgh, USA, September 2011. Available at: [https://ams.confex.com/ams/35Radar/webprogram/Manuscript/Paper191685/35RADAR\\_Maesaka.pdf](https://ams.confex.com/ams/35Radar/webprogram/Manuscript/Paper191685/35RADAR_Maesaka.pdf) [Accessed 20th December 2022].
- Mallet, C. & Barthes, L. (2009) Estimation of gamma raindrop size distribution parameters: statistical fluctuations and estimation errors. *Journal of Atmospheric and Oceanic Technology*, 26, 1572–1584.
- Marshall, J.S. & Palmer, W.M. (1948) The distribution of raindrops with size. *Journal of Meteorology*, 5, 165–166.
- Marzuki, M., Randeu, W.L., Schönhuber, M., Bringi, V.N., Kozu, T. & Shimomai, T. (2010) Raindrop size distribution parameters of distrometer data with different bin sizes. *IEEE Transactions on Geoscience Remote Sensing*, 48, 3075–3080.
- Misumi, R., Uji, Y. & Maesaka, T. (2021) Modification of raindrop size distribution due to seeder-feeder interaction observed by X-band polarimetric radar and optical disdrometer. *Atmospheric Science Letters*, 22, e1034. Available from: <https://doi.org/10.1002/asl.1034>
- Niu, S., Jia, X., Sang, J., Liu, X., Lu, C. & Liu, Y. (2010) Distributions of raindrop sizes and fall velocities in a semiarid plateau climate: convective versus stratiform rains. *Journal of Applied Meteorology and Climatology*, 49, 632–645.
- Oishi, S., Nango, S., Kajikawa, Y., Yamaura, T., Suzuki, K., Yamaguchi, K. et al. (2020) Study on drop size distribution measurement in cloud by using video sonde and SCALE-RM. *Journal of Japan Society of Civil Engineers, Series B, (Hydraulic Engineering)*, 65, 199–204.
- Prat, O.P. & Barros, A.P. (2007) A robust numerical solution of the stochastic collection-breakup equation for warm rain. *Journal of Applied Meteorology and Climatology*, 46, 1480–1497.
- Radhakrishna, B. & Rao, T.N. (2009) Multiphase raindrop size distribution observed by UHF/VHF wind profilers during the passage of a mesoscale convective system. *Monthly Weather Review*, 137, 976–990.
- Rauber, R.M. & Nesbitt, S.W. (2018) *Radar meteorology: a first course*. Hoboken, New Jersey: John Wiley & Sons.
- Rutledge, S.A. & Hobbs, P.V. (1983) The mesoscale and microscale structure and organization of clouds and precipitation in mid-latitude cyclones. VIII: a model for the “seeder-feeder” process in warm-frontal rainbands. *Journal of the Atmospheric Sciences*, 40, 1185–1206.
- Seela, B.K., Janapati, J., Lin, P.-L., Reddy, K.K., Shirooka, R. & Wang, P. K. (2017) A comparison study of summer season raindrop size distribution between Palau and Taiwan, two islands in western pacific. *Journal of Geophysical Research. Atmospheres*, 122, 11787–11805.
- Sheppard, B.E. & Joe, P.I. (1994) Comparison of raindrop size distribution measurements by a Joss-Waldvogel disdrometer, a PMS 2DG spectrometer, and a POSS doppler radar. *Journal of Atmospheric and Oceanic Technology*, 11, 874–887.
- Shusse, Y., Nakagawa, K., Takahashi, N., Satoh, S. & Iguchi, T. (2009) Characteristics of polarimetric radar variables in three types of rainfalls in a Baiu front event over the East China Sea. *Journal of the Meteorological Society of Japan*, 87, 865–875.
- Thurai, M., Bringi, V., Wolff, D., Marks, D. & Pabla, C. (2021) Testing the drop-size distribution-based separation of stratiform and convective rain using radar and disdrometer data from a mid-latitude coastal region. *Atmosphere*, 12, 392. Available from: <https://doi.org/10.3390/atmos12030392>
- Thurai, M. & Bringi, V.N. (2018) Application of the generalized gamma model to represent the full rain drop size distribution spectra. *Journal of Applied Meteorology and Climatology*, 57, 1197–1210.

- Tokay, A., Bashor, P.G., Habib, E. & Kasparis, T. (2008) Raindrop size distribution measurements in tropical cyclones. *Monthly Weather Review*, 136, 1669–1685.
- Tokay, A., Kruger, A. & Krajewski, W.F. (2001) Comparison of drop size distribution measurements by impact and optical disdrometers. *Journal of Applied Meteorology and Climatology*, 40, 2083–2097.
- Tokay, A., Petersen, W.A., Gatlin, P. & Wingo, M. (2013) Comparison of raindrop size distribution measurements by collocated disdrometers. *Journal of Atmospheric and Oceanic Technology*, 30, 1672–1690.
- Tokay, A. & Short, D.A. (1996) Evidence from tropical raindrop spectra of the origin of rain from stratiform versus convective clouds. *Journal of Applied Meteorology and Climatology*, 35, 355–371.
- Ulbrich, C.W. (1983) Natural variations in the analytical form of the raindrop size distribution. *Journal of Applied Meteorology and Climatology*, 22, 1764–1775.
- Virtanen, P., Gommers, R., Oliphant, T.E., Haberland, M., Reddy, T., Cournapeau, D. et al. (2020) SciPy 1.0: fundamental algorithms for scientific computing in python. *Nature Methods*, 17, 261–272.
- Wu, Y. & Liu, L. (2017) Statistical characteristics of raindrop size distribution in the Tibetan plateau and southern China. *Advances in Atmospheric Sciences*, 34, 727–736.

**How to cite this article:** Okazaki, M., Oishi, S., Awata, Y., Yanase, T., & Takemi, T. (2023). An analytical representation of raindrop size distribution in a mixed convective and stratiform precipitating system as revealed by field observations. *Atmospheric Science Letters*, 24(6), e1155. <https://doi.org/10.1002/asl.1155>